European Journal of Radiology 83 (2014) 1144–1151

European Journal of Radiology

journal homepage: www.elsevier.com/locate/ejrad

Whole-body-MR imaging including DWIBS in the work-up of patients with head and neck squamous cell carcinoma: A feasibility study

Daniel P. Noij[a,*], Els J. Boerhout[a], Indra C. Pieters-van den Bos[a], Emile F. Comans[a], Daniela Oprea-Lager[a], Rinze Reinhard[a], Otto S. Hoekstra[a], Remco de Bree[b], Pim de Graaf[a], Jonas A. Castelijns[a]

[a] Department of Radiology & Nuclear Medicine, VU University Medical Center, De Boelelaan 1117, PO Box 7057, 1007 MB Amsterdam, The Netherlands[1]
[b] Department Otolaryngology/Head and Neck Surgery, VU University Medical Center, De Boelelaan 1117, PO Box 7057, 1007 MB Amsterdam, The Netherlands[2]

ARTICLE INFO

Article history:
Received 31 October 2013
Received in revised form 17 March 2014
Accepted 21 March 2014

Keywords:
Diffusion magnetic resonance imaging
Head and neck neoplasms
Second primary neoplasms
Positron-emission tomography
Feasibility studies

ABSTRACT

Objectives: To assess the feasibility of whole-body magnetic resonance imaging (WB-MRI) including diffusion-weighted whole-body imaging with background-body-signal-suppression (DWIBS) for the evaluation of distant malignancies in head and neck squamous cell carcinoma (HNSCC); and to compare WB-MRI findings with ^{18}F-fluorodeoxyglucose positron emission tomography/computed tomography (^{18}F-FDG-PET/CT) and chest-CT.

Methods: Thirty-three patients with high risk for metastatic spread (26 males; range 48–79 years, mean age 63 ± 7.9 years (mean ± standard deviation) years) were prospectively included with a follow-up of six months. WB-MRI protocol included short-TI inversion recovery and T1-weighted sequences in the coronal plane and half-fourier acquisition single-shot turbo spin-echo T2 and contrast-enhanced-T1-weighted sequences in the axial plane. Axial DWIBS was reformatted in the coronal plane. Interobserver variability was assessed using weighted kappa and the proportion specific agreement (PA).

Results: Two second primary tumors and one metastasis were detected on WB-MRI. WB-MRI yielded seven clinically indeterminate lesions which did not progress at follow-up. The metastasis and one second primary tumor were found when combining ^{18}F-FDG-PET/CT and chest-CT findings. Interobserver variability for WB-MRI was $\kappa = 0.91$ with PA ranging from 0.82 to 1.00. For ^{18}F-FDG-PET/CT κ could not be calculated due to a constant variable in the table and PA ranged from 0.40 to 0.99.

Conclusions: Our WB-MRI protocol with DWIBS is feasible in the work-up of HNSCC patients for detection and characterization of distant pathology. WB-MRI can be complementary to ^{18}F-FDG-PET/CT, especially in the detection of non ^{18}F-FDG avid second primary tumors.

1. Introduction

In head and neck squamous cell carcinoma (HNSCC) patients, 2–18% present with clinically identified distant spread of disease, while autopsy incidences have been reported to be up to 57% [1]. Only palliative treatment remains when distant metastases are present in patients with HNSCC. Therefore, efforts should be made to detect distant metastases and avoid futile treatment.

Screening for distant metastases is currently done on a routine basis by means of ^{18}F-fluorodeoxyglucose positron emission tomography/computed tomography (^{18}F-FDG-PET/CT) in combination with a diagnostic chest-CT in patients at high risk of developing distant metastases. Most metastases or second primary tumors (SPT) develop within 15 months after the end of treatment with curative intent, despite negative screening on ^{18}F-FDG-PET/CT. Since false negative rates are up to 50%, room for improvement remains [1–5].

Due to several technical improvements, it is now clinically feasible to perform high-resolution whole-body magnetic resonance imaging (WB-MRI) protocols in less than one hour. In HNSCC patients, WB-MRI showed a promising role for the evaluation of

* Corresponding author. Tel.: +31 204443047; fax: +31 204442831.
E-mail addresses: d.noij@vumc.nl, daannoij@gmail.com (D.P. Noij), e.boerhout@vumc.nl (E.J. Boerhout), i.pieters@vumc.nl (I.C. Pieters-van den Bos), efi.comans@vumc.nl (E.F. Comans), d.oprea-lager@vumc.nl (D. Oprea-Lager), r.reinhard@vumc.nl (R. Reinhard), os.hoekstra@vumc.nl (O.S. Hoekstra), r.debree@vumc.nl (R. de Bree), p.degraaf@vumc.nl (P. de Graaf), j.castelijns@vumc.nl (J.A. Castelijns).
[1] Tel.: +31 20 4442863.
[2] Tel.: +31 20 4443689.

http://dx.doi.org/10.1016/j.ejrad.2014.03.019
0720-048X/

Table 1
Patient characteristics of 33 HNSCC patients at whole-body MR imaging.

n	Sex	Age	Location	Recurrence	TNM	Previous treatment
1	Male	58	Hypopharynx	Locoregional recurrence	T4N3	Chemoradiation
2	Male	68	Hypopharynx	Second primary tumor	T4N2	CO_2 laser excision
3	Male	57	Larynx	Primary tumor	T4N0	–
4	Male	57	Oropharynx	Primary tumor	T2N2	–
5	Female	69	Oropharynx	Locoregional recurrence	T3N2	Chemoradiation
6	Female	73	Larynx	Locoregional recurrence	T4N2	Excision + neck dissection + chemoradiation
7	Male	58	Oropharynx + oropharynx	Primary tumors	T2N1 + T2N1	–
8	Male	74	Nasopharynx	Second primary tumor	T1N2	Radiotherapy + excision + neck dissection + postoperative radiotherapy
9	Male	48	Oropharynx	Primary tumor	T4N2	–
10	Male	55	Oropharynx	Second primary tumor	T3N1	Neck dissection + radiotherapy
11	Male	63	Oropharynx	Primary tumor	T3N2	–
12	Male	65	Oral cavity	Locoregional recurrence	T1N0	Excision + neck dissection + radiotherapy
13	Male	70	Oropharynx	Locoregional recurrence	T2N1	Radiotherapy
14	Male	64	Hypopharynx	Primary tumor	T2N2	–
15	Male	59	Larynx	Locoregional recurrence	T2N2	Chemoradiation + excision
16	Male	62	Hypopharynx + oropharynx	Locoregional recurrence	T3N2 + T2N2	Chemoradiation
17	Female	67	Oral cavity	Second primary tumor	T4N0	Excision + neck dissection
18	Male	59	Tongue	Locoregional recurrence	T3N0	Radiotherapy
19	Male	75	Hypopharynx	Second primary tumor	T3N0	Radiotherapy
20	Male	57	Oral cavity	Second primary tumor	T2N0	Excision + neck dissection + radiotherapy
21	Male	50	Oropharynx	Primary tumor	T4N2	–
22	Female	51	Larynx	Locoregional recurrence	T2N0	Radiotherapy
23	Female	69	Oropharynx	Locoregional recurrence	T2N0	Chemoradiation
24	Male	61	Oropharynx	Primary tumor	T1N2	Radiotherapy + excision + neck dissection
25	Male	63	Oropharynx	Third primary	T3N0	–
26	Female	52	Larynx	Locoregional recurrence	T2N2	Chemoradiation
27	Male	59	Oropharynx	Primary tumor	T3N2	–
28	Male	66	Oropharynx	Primary tumor	T2N2	–
29	Male	59	Oropharynx	Primary tumor	T1N2	–
30	Male	66	Oral cavity	Recurrence	T2N0	Radiotherapy + neck dissection + excision
31	Male	79	Oropharynx	Primary tumor	T4N2	–
32	Female	60	Oropharynx	Third primary	T2N0	Excision + neck dissection
33	Male	78	Oral cavity	Locoregional recurrence	T2N0	Neck dissection + postoperative radiotherapy

metastatic spread of disease despite variations in diagnostic accuracy of WB-MRI versus ^{18}F-FDG-PET/CT [6–8].

In addition to conventional WB-MRI, diffusion-weighted imaging (DW-MRI) has shown potential. In order to deal with motion artifacts, Takahara et al. developed diffusion-weighted whole-body imaging with background body signal suppression (DWIBS). This sequence allows for the acquisition of DW-MRI under free-breathing [9]. The addition of DWIBS might improve the accuracy of WB-MRI to detect distant metastases [10–12].

The reported imaging sequences as well as imaging planes are quite variable [3,4,6–8,10–18]. As the addition of either DW-MRI or contrast-enhanced (CE) sequences may improve the outcome of diagnostic interpretation, the value of these modalities needs to be clarified further. In addition, the choice of the imaging plane (e.g. axial versus coronal) has considerable effect on the duration of the scan, and potentially on the interpretation of the images as well. Therefore, tailor-made imaging protocols may optimize the performance of WB-MRI.

The purpose of our study therefore was to prospectively assess the feasibility of WB-MRI including DWIBS for the evaluation of distant malignancies in HNSCC patients with high risk factors for the presence of metastatic disease; and to compare MRI findings with ^{18}F-FDG-PET/CT and chest-CT.

2. Materials and methods

2.1. Study population

This prospective study was performed in a tertiary referral center for HNSCC between August 2009 and June 2012. Inclusion criteria comprised histopathologically proven HNSCC; planned extensive treatment with curative intent (surgery and/or radiotherapy with or without chemotherapy); planned routine screening for the presence of distant metastases by means of ^{18}F-FDG-PET/CT and chest-CT, i.e., at least one of the high risk factors for the development of distant metastases, as previously defined by De Bree et al. (clinically three or more lymph node metastases; bilateral lymph node metastases; lymph node metastases of 6 cm or larger; low jugular lymph node metastases; locoregional recurrence or second primary tumor) [5]; and an age of 18–80 years. Exclusion criteria were pregnancy and contraindications for MRI. After approval of the local institutional review board and informed consent, 33 patients were included. For more detailed patient characteristics we refer to Table 1.

Whole-body ^{18}F-FDG-PET/CT and WB-MRI were performed at random order as dictated by logistics (time difference: mean 15.8 ± 11.3 days).

2.2. Whole-body-MRI

MR imaging was performed on a 1.5T-system (Magnetom Avanto; Siemens, Erlangen, Germany), using a total imaging matrix (TIM) coil system combined with dedicated coils. WB-MRI up to the upper femora was performed with the acquisition of a T1-weighted sequence in the coronal plane; a short-tau inversion recovery (STIR) sequence in the coronal plane; an axial T2-weighted sequence covering the entire body; dedicated axial liver sequences covering the upper abdomen in the axial plane, including in- and opposed phase T1 gradient-echo (GRE).

DWIBS was acquired using with a 2D EPI sequence in the axial plane and reformatted in the coronal plane and presented with inverted signal intensity (b-value: 1000 s/mm^2; number of averages: 2; fat saturation: SPAIR; parallel imaging: GRAPPA).

After administration of 0.2 mmol/kg gadoteric acid in 17 patients (Dotarem; Guerbet, Roissy, France) and of 0.15 mmol/kg gadobutrol in 15 patients (Gadovist; Bayer Schering AG, Berlin,

Table 2
MR Imaging protocol at 1.5T used in HNSCC patients (*DW* diffusionweighted, *EPI* echo-planar imaging, *FLASH* fast low angle shot, *FS* fat saturation, *GRE* gradient echo, *HASTE* half-Fourier acquisition single-shot turbo spin-echo, *STIR* short-TI inversion recovery, *TSE* turbo spin echo, *VIBE* volumetric interpolated breath-hold).

	Sequence	Region	TR (ms)	TE (ms)	Matrix	FOV (mm)	Slices	Thickness (mm)	Flip angle	Scan time (min:s)
Pre-contrast	Cor STIR	Whole body	6000	62	320 × 224	500	31	4	150	10:00
	Cor T1 TSE	Whole body	520	9.1	320 × 256	500	31	4	150	9:00
	Ax DW-MRI-EPI	Whole body	8200	66	128 × 88	500	60	4	90	9:00
	Ax T2 TSE	Head and Neck	4750	108	448 × 252	250	28	5	180	1:41
	Ax T1 GRE	Liver	100	2.38/4.76	256 × 154	350	20	6	70	0:32
	Ax HASTE-T2	Thorax-pelvis	1000	65	256 × 165	500	20	8	150	0:22
	Ax VIBE FS	Liver	5.46	2.38	256 × 135	450	64	3	10	0:21
Postcontrast	Ax VIBE FS	Liver	5.46	2.38	256 × 135	450	64	3	10	1:30
	Ax T1 TSE	Head and Neck	755	9.5	320 × 256	250	28	5	150	1:31
	Ax FLASH 2D FS	Thorax-pelvis	202	4.76	256 × 166	500	35	6	70	0:58
									Total	34:55

Germany) dynamic contrast-enhanced fat-suppressed volumetric interpolated breath-hold (VIBE) T1-weighted sequences in the arterial and delayed venous phases and a T1-weighted sequence covering the entire body were acquired in the axial plane. One patient did not receive MR-contrast due to renal failure. An overview of the scanned anatomic regions and sequences is provided in Tables 2 and 3. Total examination time approximated 60 min, with scan time being 35 min.

2.3. ^{18}F-FDG-PET/CT

Thirty-one patients underwent a PET/low-dose CT (LD-CT) scan after a 6 h fast period and adequate hydration. The examination was performed from mid-thigh to skull vertex, 60 min after intravenous administration of 250–370 MBq ^{18}F-FDG. Scans were acquired on a Gemini TOF-64 PET/CT scanner (Philips Medical Systems, Best, The Netherlands) with an axial field of view of 18 cm. Time of flight (TOF) information was used during reconstruction. Reconstructed images had an image matrix size of 144 × 144, a pixel size of 4 mm × 4 mm and a slice thickness of 5 mm. Low-dose-CT was collected using a beam current of 30 to 50 mAs at 120 keV. CT-scans were reconstructed using an image matrix size of 512 × 512 resulting in pixel sizes of 1.17 mm × 1.17 mm and a slice thickness of 5 mm.

In two patients, examinations were performed at other institutions using Gemini TOF-64 and TOF-16 PET/CT scanners (Philips Medical Systems, Best, The Netherlands), respectively.

2.4. Chest-CT

Chest-CT-scans were performed in 32 patients in the early arterial phase on a fourth-generation CT-scanner (Somaton Plus; Siemens, Erlangen, Germany) after intravenous contrast administration (Ultravist, Bayer Schering AG, Berlin, Germany) with a reconstructed slice thickness of 5 mm. In one patient only LD-CT was performed.

Table 3
Schematic MR imaging protocol at 1.5 T used in HNSCC patients (*CE* contrast-enhanced, *DWIBS* diffusion-weighted whole-body imaging with background-body-signal-suppression, *GRE* gradient echo, *HASTE* half-Fourier acquisition single-shot turbo spin-echo, *SE* spin echo, *STIR* short-TI inversion recovery, *TSE* turbo spin echo, *VIBE* volumetric interpolated breath-hold).

TIM coil system										
Head coil 4 elements		Whole-body	Whole-body	Whole-body	Head and neck	Liver	Liver	CONTRAST	Liver	Whole-body
Neck coil 2 elements	Spine coil 24 elements	STIR coronal	SE-T1 coronal	DWIBS coronal	TSE-T2 axial	In-phase GRE-T1 axial	Pre-contrast VIBE axial		3-phase VIBE axial	CE-T1 axial
Torso coil 4 elements					Thorax - abdomen - pelvis HASTE-T2 axial	Liver Opposed-phase GRE-T1 axial				
Abdominal coil 4 elements										

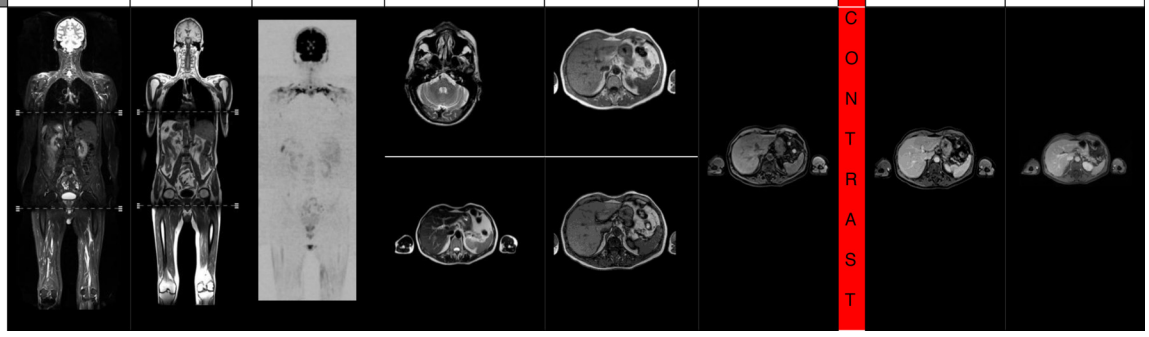

2.5. Image analysis

All readers were aware of the HNSCC diagnosis, but blinded to all other information, including the other imaging test results.

Whole-body-MRI images were analyzed for distant metastasis and SPT by two independent reviewers, with 4 and 2 years experience in WB-MRI. After separate analysis the final decision was made in consensus. The analysis consisted of two parts: (1) evaluation of all conventional sequences without DWIBS; and (2) evaluation after DWIBS was added to the conventional sequences. Overall image quality and artifacts were assessed, per sequence, on a four-point Likert scale. For image quality: 1, inadequate; 2, adequate; 3, good; 4, excellent. For artifacts: 1, none present; 2, irrelevant; 3, diagnostically relevant; 4, marked. To complete the assessment of image quality the sequences that best depicted the pathology were selected. Although the primary goal was screening for distant metastases, SPT and incidental findings were also registered. Based on all MRI findings the likelihood of metastasis and/or SPT was scored on a three-point Likert scale: 1, yes; 2, clinically indeterminate, 3 = no. The presence of malignancy was suspected on conventional WB-MRI in focal lesions with different signal intensities compared to the surrounding tissue. On the DWIBS malignancy was suspected in case of abnormal signal intensity in focal lesions.

At first, ^{18}F-FDG-PET/CT images were analyzed independently for distant metastasis and SPT by two reviewers with 12 and 4 years' experience in PET analysis. Again the final decision was made in consensus. The likelihood of metastasis and/or SPT was scored on a three-point Likert scale: 1, yes; 2, clinically indeterminate; 3, no. Again the primary goal was screening on distant metastases, but SPT and other abnormalities were also registered. Lesions were characterized as suspicious for malignancy based on increased ^{18}F-FDG uptake, incompatible with physiological ^{18}F-FDG distribution, within structures with an anatomical substrate on the (LD-)CT. Chest-CT was analyzed for distant metastasis and SPT by a radiologist with 7 years of experience. The likelihood of metastasis and/or SPT was scored on a three-point Likert scale: 1, yes; 2, clinically indeterminate; 3, no.

When the presence of metastasis and/or SPT based on imaging was classified as 'yes' or 'clinically indeterminate', the final diagnosis regarding the presence of malignancy was based on histopathology or progression at six months of clinical follow-up (i.e., clinical assessment in the outpatient clinic every two months).

2.6. Statistical analysis

Interobserver variability for WB-MRI and ^{18}F-FDG-PET/CT was calculated with weighted kappa using Stata (version 11.2; College Station, TX, USA) and with proportion specific agreement using Microsoft Excel (Microsoft Office 2010, Microsoft, Redmond, WA, USA) [19]. For the interpretation of weighted kappa the following cut-off values are used: $\leq$0.20 = poor, 0.21–0.40 = fair, 0.41–0.60 = moderate, 0.61–0.80 = substantial, 0.81–1.00 = very good [20]. The proportion specific agreement consists of two parts: positive agreement (PA) and negative agreement (NA). These two numbers express the agreement on positive and negative ratings respectively. Two sets of positive and negative ratings are calculated to deal with the 'clinically indeterminate' category regarding the presence of malignancy. In the first set clinically indeterminate is recoded into 'yes': $PA_{\text{clinically indeterminate = yes}}$ and $NA_{\text{clinically indeterminate = yes}}$. In the second set 'clinically indeterminate' is recoded into 'no': $PA_{\text{clinically indeterminate = no}}$ and $NA_{\text{clinically indeterminate = no}}$.

3. Results

3.1. MRI quality

One patient did not receive MR-contrast due to renal failure. All other patients completed the entire protocol. Median image quality scores of the MR sequences were: 4 (range, 3–4) for coronal T1; 4 (range, 2–4) for coronal STIR; 3 (range, 3–4) for axial T2; 3 (range, 1–4) for axial T1 with contrast and 4 (range, 2–4) for DWIBS, and for artifacts: 1 (range, 1–2) for coronal T1; 2 (range, 1–3) for coronal STIR; 1 (range, 1–2) for axial T2; 1 (range, 1–4) for axial T1 with contrast and 1 (range, 1–3) for DWIBS. The coronal STIR was indicated to be most informative in 19 patients, coronal DWIBS in 24 patients and axial T2 in 17 patients by both reviewers.

3.2. Comparison between WB-MRI, ^{18}F-FDG-PET/CT and chest-CT

One patient had a distant HNSCC metastasis (lung; maximum axial diameter: 8 mm) (Fig. 1) and two had SPT (renal cell carcinoma (RCC); maximum axial diameter: 80 mm, and a neuroendocrine tumor with liver metastases; maximum axial diameter: 20 mm) (Fig. 2). On WB-MRI, without DWIBS, this metastasis was suspected and both SPTs were found. On DWIBS these three lesions all showed diffusion restriction, this confirmed the presence of malignancy. In another patient DWIBS aided in favor of the correct final diagnosis: the addition of DWIBS changed the conclusion regarding the presence of malignancy from 'clinically indeterminate' to 'no' in a benign cervical bone lesion. Seven lesions on WB-MRI including DWIBS were classified as clinically indeterminate: two vertebral lesions (one had a negative biopsy and both did not progress at follow-up), four thoracic lesions (all regressed at follow-up) and one pancreatic lesion (did not progress at follow-up). An adrenal lesion was correctly qualified as benign, whereas diagnostic chest-CT was equivocal. The lesion did not show ^{18}F-FDG uptake on ^{18}F-FDG-PET/CT and did not progress at follow-up. Other relevant incidental findings detected on WB-MRI were bone infarction, cholelithiasis, (old) brain infarction, scoliosis, hemochromatosis and atelectasis. WB-MRI was correctly negative in 25 patients, after the addition of DWIBS in 24 patients.

On ^{18}F-FDG-PET/CT the HNSCC lung metastasis was also detected, but not the SPTs. Two lesions, a focal lung lesion and a vertebral bone lesion, were classified as clinically indeterminate. ^{18}F-FDG-PET/CT was correctly negative in 30 patients. On chest-CT the HNSCC lung metastasis and the RCC were identified. Eight lesions were classified as clinically indeterminate: four focal lung lesions, two lymph nodes, one bone lesion and a liver lesion. None of these lesions did progress at follow-up. Chest-CT was correctly negative in 25 patients.

The clinical standard of practice (^{18}F-FDG-PET/CT and chest-CT) yielded metastasized HNSCC in one patient and RCC in another. One vertebral bone lesion remained clinically indeterminate using the clinical standard of practice. This lesion did not progress at follow-up.

The interobserver agreement for WB-MRI was very good (κ = 0.91, $PA_{\text{clinically indeterminate = yes}}$ = 0.82; $NA_{\text{clinically indeterminate = yes}}$ = 0.96; $PA_{\text{clinically indeterminate = no}}$ = 1.00 and $NA_{\text{clinically indeterminate = no}}$ = 1.00). For ^{18}F-FDG-PET/CT weighted kappa could not be calculated. This is because the table contained a constant variable, which made it impossible to calculate weighted kappa. Proportion specific agreement was: $PA_{\text{clinically indeterminate = yes}}$ = 0.40; $NA_{\text{clinically indeterminate = yes}}$ = 0.98; $PA_{\text{clinically indeterminate = no}}$ = 0.67 and $NA_{\text{clinically indeterminate = no}}$ = 0.99.

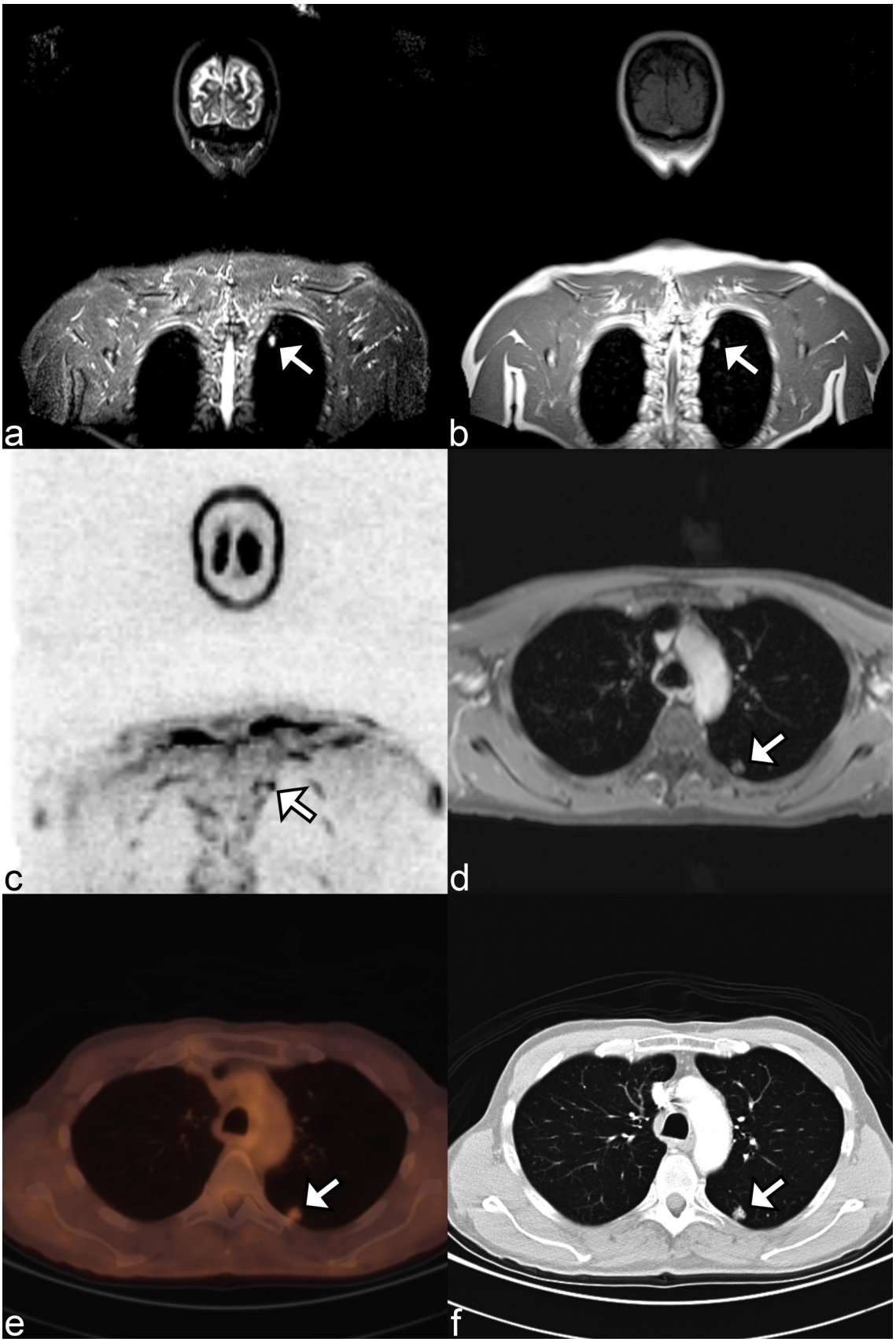

Fig. 1. Coronal and axial images in a 62-year old male with a lung metastasis in the apex of the left lower lobe (*arrow*). (a) Coronal STIR, (b) coronal T1, (c) DWIBS, (d) axial contrast-enhanced T1, (e) axial fused ^{18}F-FDG-PET/CT and (f) axial chest-CT. Mainly due to diffusion-restriction on the coronal DWIBS this lesion is suspected to be malignant. The lesion demonstrates ^{18}F-FDG uptake and on chest-CT a solitary non-calcified nodule is seen.

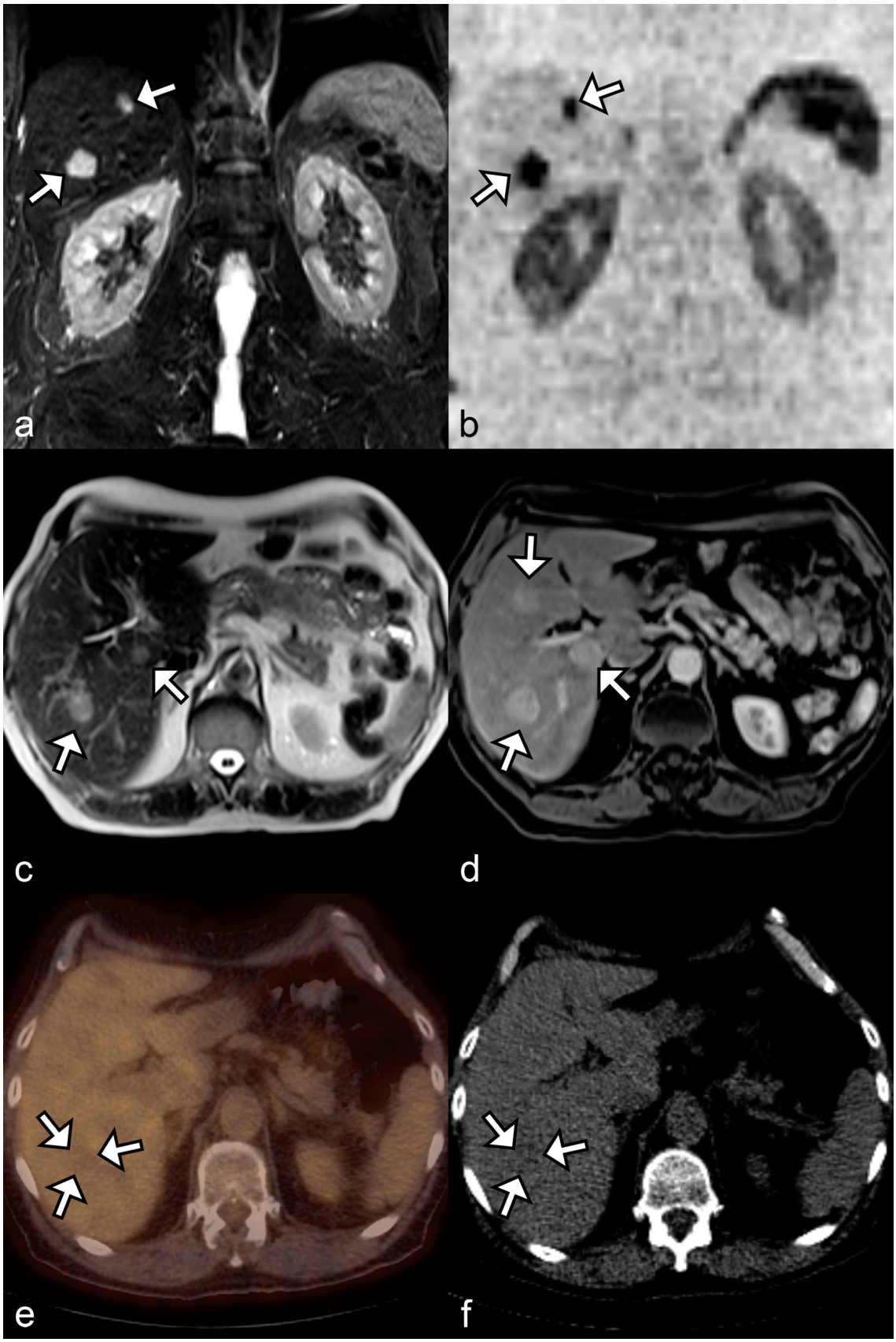

Fig. 2. Images of a focal liver lesion (*arrows*) in a 68-year old male (multiple other lesions with identical characteristics not shown). (a) Coronal STIR, (b) DWIBS, (c) axial HASTE-T2, (d) axial contrast-enhanced-T1-weighted VIBE in the arterial phase, (e) axial fused ^{18}F-FDG-PET/CT and (f) axial LD-CT. Based on MR imaging findings this lesion is suspicious of malignancy, with neuroendocrine liver metastases as first differential option. This has been confirmed after biopsy. The high signal of the spleen on DWIBS can be considered physiological. The lesion is outside the field of view of the diagnostic chest-CT. No uptake of ^{18}F-FDG is seen. On low-dose CT a minimally hypodense lesion is seen only after visual correlation with MR-images. Therefore this lesion is regarded as undetected in further data-analysis.

4. Discussion

Various WB-MRI protocols have been compared to ^{18}F-FDG-PET/CT in the work-up of patients with (suspicion of) distant metastases. In patients with colorectal and breast cancer Schmidt et al. used an imaging protocol containing coronal STIR, coronal T1 and axial CE-T1. Radiological follow-up of at least 5 months served as a standard of reference [13,14]. In both studies WB-MRI and ^{18}F-FDG-PET/CT had comparable diagnostic accuracy in detecting distant metastases. However, sensitivity and specificity of WB-MRI to detect metastatic disease were variable: 95% and 92% in breast cancer and 78% and 95% in colorectal cancer respectively. This suggests that the value of WB-MRI may depend on the type of malignancy and its metastatic pattern. Ohno et al. found the combination of conventional WB-MRI and DW-MRI to have a diagnostic accuracy comparable to ^{18}F-FDG-PET/CT for M-stage assessment in non-small cell lung cancer, using a combination of imaging, biopsy and at least 12 months of clinical follow-up as the reference standard. Sensitivity seemed to improve after the addition of DW-MRI to conventional MRI (from 60% to 70%) [18]. Heusner et al. demonstrated high sensitivity (91%), but low specificity (72%) of whole-body DW-MRI alone in the detecting breast cancer metastases. Specificity was especially compromised in lymph nodes and bone lesions [16].

Taken together, these data suggest that imaging protocols containing more MR-sequences than DW-MRI alone may be preferable. Compared to conventional DW-MRI, DWIBS has the advantage that it allows for DW-MRI during free breathing [9]. Due to background suppression small lesions are more easily detected on DWIBS [21].

In our study WB-MRI including DWIBS was superior to ^{18}F-FDG-PET/CT in the detection of SPT. In general SPTs in HNSCC mainly emerge in the head and neck area and the lungs [22]. ^{18}F-FDG uptake of RCC and neuroendocrine tumors is variable. Populations have been described where only 22% of the RCCs showed increased ^{18}F-FDG uptake [23,24]. Ng et al. performed two studies in patients with advanced HNSCC. In a study of 79 patients with advanced HNSCC, Ng et al. reported that ^{18}F-FDG-PET/CT showed a (non-significant) trend toward higher diagnostic capability than conventional WB-MRI in detecting SPT below the clavicles (4/5 vs 2/5). In another study in 150 patients with advanced HNSCC both modalities were comparable. On WB-MRI a bronchoalveolar cell carcinoma was detected, due to low ^{18}F-FDG-uptake this was interpreted as inflammation on ^{18}F-FDG-PET/CT. Using ^{18}F-FDG-PET/CT colon carcinoma was found, which was missed on WB-MRI. On both modalities another SPT in the lung was detected [8,25].

Whole-body-MRI is considerably less expensive than ^{18}F-FDG-PET/CT. If WB-MRI can replace ^{18}F-FDG-PET/CT, a substantial reduction of health costs seems to be possible. Moreover, patients undergoing WB-MRI are not exposed to radiation as by ^{18}F-FDG-PET/CT. To replace ^{18}F-FDG-PET/CT, WB-MRI needs to have at least comparable diagnostic accuracy [26]. However, the biological information provided by the level of ^{18}F-FDG uptake may carry prognostic relevance, and serial uptake measurements may serve as a predictive biomarker [27]. Hence, if the chest-CT information proves to be redundant, PET-MRI might become the method of choice for personalized therapy.

In this pilot study we used a combination of STIR and T1 in the coronal plane combined with T2 and dedicated liver sequences in the axial plane. DWIBS was acquired in the axial plane and reformatted in the coronal plane. By using this combination we demonstrated the feasibility of WB-MRI not only to detect benign and malignant lesions, but also characterize them (e.g. hemangiomas, renal cysts, bone infarction and hemochromatosis). In our study population WB-MRI allowed for the detection of two non ^{18}F-FDG avid malignancies. Whole-body MRI yielded seven clinically indeterminate lesions. In one of these lesions biopsy was performed. None of the clinically indeterminate lesions did progress at follow-up. The addition of DWIBS aided in making the correct final diagnosis of a HNSCC lung metastasis and a benign cervical bone lesion. Particular in bone and thoracic lesions WB-MRI including DWIBS remained clinically inconclusive. On ^{18}F-FDG-PET/CT small thoracic lesions were difficult to deal with and for chest-CT lung nodules and mediastinal lymph nodes were challenging to characterize.

We believe that there is a learning curve in the evaluation of WB-MRI including DWIBS. The addition of DWIBS to WB-MRI protocols allows for fast image interpretation since it enables distinguishment of malignant from benign tissue “at-a-glance” [28]. The use of coronal images requires additional training as most radiologists are more familiar with axial images. Incidental findings are more frequently present than on ^{18}F-FDG-PET/CT due to the higher soft tissue detail on WB-MRI. Therefore some experience in WB-MRI is necessary to deal with them properly.

Our study had some limitations. First, the incidence of distant metastases was lower than would be expected according to our inclusion criteria as defined by de Bree et al. [5]; only one patient had a distant metastasis and two patients demonstrated SPTs. Some patients with high suspicion of distant metastases visualized on ^{18}F-FDG-PET-CT refrained from WB-MRI. In the future this could be prevented by performing all imaging on the same day. Other patients refrained from WB-MRI due to claustrophobia. This limited the possibilities for statistical analysis. Second, because this is a pilot study, the number of patients was limited. Therefore it is necessary to prospectively validate this MR-protocol in a larger population.

5. Conclusions

The presented WB-MRI protocol with DWIBS is feasible in the work-up of patients with advanced HNSCC for the detection and characterization of distant pathology; it allowed for the detection of non ^{18}F-FDG avid malignancies and can therefore be complementary to ^{18}F-FDG-PET/CT.

Conflict of interest

None.

References

[1] de Bree R, Haigentz M, Silver CE, Paccagnella D, Hamoir M, Hartl DM, et al. Distant metastases from head and neck squamous cell carcinoma. Part II. Diagnosis. Oral Oncol 2012;48(9):780–6.
[2] Senft A, de Bree R, Hoekstra OS, Kuik DJ, Golding RP, Oyen WJ, et al. Screening for distant metastases in head and neck cancer patients by chest CT or whole body FDG-PET: a prospective multicenter trial. Radiother Oncol 2008;87(2):221–9.
[3] Ng SH, Chan SC, Liao CT, Chang JT, Ko SF, Wang HM, et al. Distant metastases and synchronous second primary tumors in patients with newly diagnosed oropharyngeal and hypopharyngeal carcinomas: evaluation of (18)F-FDG PET and extended-field multi-detector row CT. Neuroradiology 2008;50(11):969–79.
[4] Kim SY, Roh JL, Yeo NK, Kim JS, Lee JH, Choi SH, et al. Combined 18F-fluorodeoxyglucose-positron emission tomography and computed tomography as a primary screening method for detecting second primary cancers and distant metastases in patients with head and neck cancer. Ann Oncol 2007;18(10):1698–703.
[5] de Bree R, Deurloo EE, Snow GB, Leemans CR. Screening for distant metastases in patients with head and neck cancer. Laryngoscope 2000;110(3 Pt 1):397–401.
[6] Fruehwald-Pallamar J, Czerny C, Mayerhoefer ME, Halpern BS, Eder-Czembirek C, Brunner, et al. Functional imaging in head and neck squamous cell carcinoma: correlation of PET/CT and diffusion-weighted imaging at 3 T. Eur J Nucl Med Mol Imaging 2011;38(6):1009–19.
[7] Chan SC, Wang HM, Yen TC, Lin CY, Chin SC, Liao CT, et al. 18F-FDG PET/CT and 3.0-T whole-body MRI for the detection of distant metastases and second primary tumours in patients with untreated oropharyngeal/hypopharyngeal carcinoma: a comparative study. Eur J Nucl Med Mol Imaging 2011;38(9):1607–19.

[8] Ng SH, Chan SC, Yen TC, Chang JT, Liao CT, Ko SF, et al. Pretreatment evaluation of distant-site status in patients with nasopharyngeal carcinoma: accuracy of whole-body MRI at 3-T and FDG-PET-CT. Eur Radiol 2009;19(12):2965–76.
[9] Takahara T, Imai Y, Yamashita T, Yasuda S, Nasu S, Van Cauteren M. Diffusion weighted whole body imaging with background body signal suppression (DWIBS): technical improvement using free breathing, STIR and high resolution 3D display. Radiat Med 2004;22(4):275–82.
[10] Mürtz P, Krautmacher C, Träber F, Gieseke J, Schild HH, Willinek WA. Diffusion-weighted whole-body MR imaging with background body signal suppression: a feasibility study at 3.0 T. Eur Radiol 2007;17(12):3031–7.
[11] Komori T, Narabayashi I, Matsumura K, Matsuki M, Akagi H, Ogura Y, et al. 2-[Fluorine-18]-fluoro-2-deoxy-D-glucose positron emission tomography/computed tomography versus whole-body diffusion-weighted MRI for detection of malignant lesions: initial experience. Ann Nucl Med 2007;21(4):209–15.
[12] Sommer G, Klarhöfer M, Lenz C, Scheffler K, Bongartz G, Winter L. Signal characteristics of focal bone marrow lesions in patients with multiple myeloma using whole body T1w-TSE, T2w-STIR and diffusion-weighted imaging with background suppression. Eur Radiol 2011;21(4):857–62.
[13] Schmidt GP, Baur-Melnyk A, Haug A, Heinemann V, Bauerfeind I, Reiser MF, et al. Comprehensive imaging of tumor recurrence in breast cancer patients using whole-body MRI at 1.5 and 3 T compared to FDG-PET-CT. Eur J Radiol 2008;65(1):47–58.
[14] Schmidt GP, Baur-Melnyk A, Haug A, Utzschneider S, Becker CR, Tiling R, et al. Whole-body MRI at 1.5 T and 3 T compared with FDG-PET-CT for the detection of tumour recurrence in patients with colorectal cancer. Eur Radiol 2009;19(6):1366–78.
[15] Fischer MA, Nanz D, Hany T, Reiner CS, Stolzmann P, Donati OF, et al. Diagnostic accuracy of whole-body MRI/DWI image fusion for detection of malignant tumours: a comparison with PET/CT. Eur Radiol 2011;21(2):246–55.
[16] Heusner TA, Kuemmel S, Koeninger A, Hamami ME, Hahn S, Quinsten A, et al. Diagnostic value of diffusion-weighted magnetic resonance imaging (DWI) compared to FDG PET/CT for whole-body breast cancer staging. Eur J Nucl Med Mol Imaging 2010;37(6):1077–86.
[17] Brauck K, Zenge MO, Vogt FM, Quick HH, Stock F, Trarbach T, et al. Feasibility of whole-body MR with T2- and T1-weighted real-time steady-state free precession sequences during continuous table movement to depict metastases. Radiology 2008;246(3):910–6.
[18] Ohno Y, Koyama H, Onishi Y, Takenaka D, Nogami M, Yoshikawa T, et al. Non-small cell lung cancer: whole-body MR examination for M-stage assessment – utility for whole-body diffusion-weighted imaging compared with integrated FDG PET/CT. Radiology 2008;248(2):643–54.
[19] de Vet HC, Mokkink LB, Terwee CB, Hoekstra OS, Knol DL. Clinicians are right not to like Cohen's κ. BMJ 2013;346:f2125.
[20] Landis JR, Koch GG. The measurement of observer agreement for categorical data. Biometrics 1977;33(1):159–74.
[21] Kwee TC, Takahara T, Ochiai R, Nievelstein RA, Luijten PR. Diffusion-weighted whole-body imaging with background body signal suppression (DWIBS): features and potential applications in oncology. Eur Radiol 2008;18(9):1937–52.
[22] Morris LG, Sikora AG, Patel SG, Hayes RB, Ganly I. Second primary cancers after an index head and neck cancer: subsite-specific trends in the era of human papillomavirus-associated oropharyngeal cancer. J Clin Oncol 2011;29(6):739–46.
[23] Oyama N, Ito H, Takahara N, Miwa Y, Akino H, Kudo T, et al. Diagnosis of complex renal cystic masses and solid renal lesions using PET imaging: comparison of 11C-acetate and 18F-FDG PET imaging. Clin Nucl Med 2014;39(3):e208–14.
[24] Jadvar H. Hepatocellular carcinoma and gastroenteropancreatic neuroendocrine tumors: potential role of other positron emission tomography radiotracers. Semin Nucl Med 2012;42(4):247–54.
[25] Ng SH, Chan SC, Yen TC, Liao CT, Lin CY, Tung-Chieh Chang J, et al. PET/CT and 3-T whole-body MRI in the detection of malignancy in treated oropharyngeal and hypopharyngeal carcinoma. Eur J Nucl Med Mol Imaging 2011;38(6):996–1008.
[26] Plathow C, Walz M, Lichy MP, Aschoff P, Pfannenberg C, Bock H, et al. Cost considerations for whole-body MRI and PET/CT as part of oncologic staging. Radiologe 2008;48(4):384–96.
[27] Quarles van Ufford HM, van Tinteren H, Stroobants SG, Riphagen II, Hoekstra OS. Added value of baseline 18F-FDG uptake in serial 18F-FDG PET for evaluation of response of solid extracerebral tumors to systemic cytotoxic neoadjuvant treatment: a meta-analysis. J Nucl Med 2010;51(10):1507–16.
[28] Padhani A, Koh D. Whole-body diffusion-weighted MR imaging in cancer: current status and research directions. Radiology 2011;261(3):700–18.